PHYSICAL REVIEW D **92,** 115009 (2015)

Sbottom discovery via mixed decays at the LHC

Tao Han,[1,2,*] Shufang Su,[3,2,†] Yongcheng Wu,[2,‡] Bin Zhang,[2,§] and Huanian Zhang[3,‖]

[1]*PITT PACC, Department of Physics and Astronomy, University of Pittsburgh, Pittsburgh, Pennsylvania 15260, USA*

[2]*Department of Physics, Tsinghua University, Beijing 100086, China*

[3]*Department of Physics, University of Arizona, Tucson, Arizona 85721, USA*

(Received 1 September 2015; published 14 December 2015)

In the search for the bottom squark (sbottom) in supersymmetry (SUSY) at the LHC, the common practice has been to assume a 100% decay branching fraction for a given search channel. In realistic minimal supersymmetric Standard Model scenarios, there are often more than one significant decay modes to be present, which significantly weaken the current sbottom search limits at the LHC. On the other hand, the combination of the multiple decay modes offers alternative discovery channels for sbottom searches. In this paper, we present the sbottom decays in a few representative mass parameter scenarios. We then analyze the sbottom signal for the pair production in QCD with one sbottom decaying via $\tilde{b} \to b\chi_1^0$, $b\chi_2^0$, and the other one decaying via $\tilde{b} \to t\chi_1^\pm$. With the gaugino subsequent decaying to gauge bosons or a Higgs boson $\chi_2^0 \to Z\chi_1^0$, $h\chi_1^0$ and $\chi_1^\pm \to W^\pm\chi_1^0$, we study the reach of those signals at the 14 TeV LHC with 300 fb^{-1} integrated luminosity. For a left-handed bottom squark, we find that a mass up to 920 GeV can be discovered at 5σ significance for 250 GeV $< m_{\chi_1^0} <$ 350 GeV, or excluded up to 1050 GeV at the 95% confidence level for the h channel ($\mu > 0$); similarly, it can be discovered up to 840 GeV, or excluded up to 900 GeV at the 95% confidence level for the Z channel ($\mu < 0$). The top squark reach is close to that of the bottom squark. The sbottom and stop signals in the same SUSY parameter scenario are combined to obtain the optimal sensitivity, which is about 150 GeV better than the individual reach of the sbottom or stop. For a right-handed bottom squark with the $\tilde{b}\tilde{b}^* \to b\chi_1^0, t\chi_1^\pm$ channel, we find that the sbottom mass up to 880 GeV can be discovered at 5σ significance, or excluded up to 1060 GeV at the 95% confidence level.

DOI: 10.1103/PhysRevD.92.115009 PACS numbers: 12.60.Jv, 14.80.Ly

I. INTRODUCTION

The outstanding performance of the Large Hadron Collider (LHC) at CERN had led to the milestone discovery of the Higgs boson predicted by the Standard Model (SM). High energy physics has thus entered a new era in understanding the nature of electroweak symmetry breaking. The "naturalness" argument for the Higgs boson mass implies new physics associated with the SM Higgs sector not far above the TeV scale [1–3]. The LHC Run-2 with higher energy and higher luminosity will certainly extend the horizon to seek for new physics. Among the new physics scenarios, the weak scale supersymmetry (SUSY) remains to be the most attractive option because of the accommodation for a light Higgs boson, the natural dark matter candidate, and the possibility for gauge coupling unification. In preparing to exploit a large amount of the incoming data from the LHC experiments, it is thus of priority to embrace the SUSY searches in a comprehensive way.

While the top squark (stop $\tilde{t}$) sector might be the most relevant supersymmetric partner in connection to the Higgs physics given the large top Yukawa coupling, the bottom squark (sbottom $\tilde{b}$) sector is also of great interest. The left-handed sbottom mass is related to the left-handed stop mass since they are controlled by the same soft SUSY breaking mass parameter [4,5]. In the region of the large ratio of the Higgs vacuum expectation values, $\tan\beta = v_2/v_1$, the bottom Yukawa coupling is large, and there could be large corrections to the Higgs physics from the sbottom sector as well [6]. Although the LHC program has been carrying out a rather broad and impressive SUSY search plan, many searches are still under strong assumptions for the sake of simplicity. The current sbottom search mainly focuses on the direct decay to the lightest supersymmetric particle (LSP) $\tilde{b} \to b\chi_1^0$, with $b\bar{b} + \not{E}_T$ being the dominant search channel. With the data collected at the LHC 7 and 8 TeV, a sbottom with mass up to 700 GeV has been excluded in this channel [7–9]. Even in the parameter space with highly degenerate sbottom and LSP masses [10–14], a sbottom is excluded with mass up to about 255 GeV [9]. Other decay channels including the cascade decay via the next-lightest supersymmetric particle (NLSP) $\tilde{b} \to b\chi_2^0 \to bh\chi_1^0$, $bZ\chi_1^0$ [15,16] and $\tilde{b} \to tW\chi_1^0$ [16–19] have also been considered

*than@pitt.edu
†shufang@email.arizona.edu
‡wuyongcheng12@mails.tsinghua.edu.cn
§zb@mail.tsinghua.edu.cn
‖fantasyzhn@email.arizona.edu

with a 100% branching fraction each, with considerably weaker limits.

In realistic minimal supersymmetric Standard Model (MSSM) scenarios, there are often more than one significant decay modes to be present. Two prominent examples stand out: A left-handed sbottom in the Wino-NLSP scenario may have a decay $\tilde{b} \to b\chi_2^0$ with a branching fraction as high as 30%–40%, along with the leading decay $\tilde{b} \to t\chi_1^\pm$. Similarly, a right-handed sbottom in the Higgsino-NLSP scenario may have the leading decay mode $\tilde{b} \to b\chi_1^0$ with a branching fraction only 40%–60%, along with a subleading decay $\tilde{b} \to t\chi_1^\pm$ of 20%–30%. Those additional channels dilute the leading signals currently being searched for at the LHC, and they significantly weaken the sbottom search limits when assuming a 100% branching fraction for a given search channel. On the other hand, the combination of the multiple decay modes offers alternative discovery channels for sbottom searches, which must be properly taken into account.

In this paper, we present the sbottom decays in a few representative SUSY mass scenarios. We then analyze the sbottom pair production signal with one sbottom decaying via $\tilde{b} \to b\chi_1^0, b\chi_2^0$, and the other one decaying via $\tilde{b} \to t\chi_1^\pm$. With the subsequent decay of $\chi_2^0 \to Z\chi_1^0$, $h\chi_1^0$ and $\chi_1^\pm \to W^\pm\chi_1^0$, we study the reach of those signals at the 14 TeV LHC with 300 fb^{-1} integrated luminosity. Because of the similarity of the final state signatures and potential correlation of the left-handed soft mass, the sbottom and stop signals are combined to obtain the optimal sensitivity for the same SUSY parameter region. We find for a left-handed bottom squark, a mass up to 920 GeV can be discovered at 5σ significance for 250 GeV $< m_{\chi_1^0} <$ 350 GeV, or excluded up to 1050 GeV at the 95% confidence level for the h channel ($\mu > 0$); similarly, the bottom squark can be discovered up to 840 GeV, or excluded up to 900 GeV at the 95% confidence level for the Z channel ($\mu < 0$); the top squark reach is close to that of the bottom squark. The sbottom and stop signals in the same SUSY parameter scenario are combined to obtain the optimal sensitivity, which is about 150 GeV better than the individual reach of the sbottom or stop. For a right-handed bottom squark with the channel $\tilde{b}\tilde{b}^* \to b\chi_1^0$, $t\chi_1^\pm \to tbW + \not{E}_T$, we find that a mass up to 880 GeV can be discovered at 5σ significance, or excluded up to 1060 GeV at the 95% confidence level.

The rest of the paper is organized as follows. In Sec. II, we briefly present the sbottom sector in the MSSM and introduce the mass and mixing parameters. We then calculate the sbottom decays for various neutralino/chargino mass spectra. Assuming one decay channel dominant at a time, we summarize the current LHC stop and sbottom search results from both ATLAS and CMS experiments. In Sec. III, we investigate the reach of the sbottom signal with mixed decay channels at the 14 TeV LHC. We combine the left-handed sbottom and stop signals for the same SUSY parameter region. In Sec. IV, we summarize our results.

II. MSSM SBOTTOM SECTOR

We work in the MSSM and focus primarily on the third generation squark sector. We decouple other SUSY particles: the gluino, sleptons, and the first two generations of squarks. We also decouple the non-SM Higgs particles by setting M_A large. Besides the third generation squarks, the other relevant SUSY states are a Bino (with a soft SUSY breaking mass M_1), Winos (with a soft SUSY breaking mass M_2), and Higgsinos (with bilinear Higgs mass parameter μ). Up on the mass diagonalization, they form neutralinos ($\chi_{1,2,3,4}^0$) and charginos ($\chi_{1,2}^\pm$).

A. The sbottom sector

The gauge eigenstates for the the third generation squark sector are $\tilde{t}_L, \tilde{b}_L, \tilde{t}_R, \tilde{b}_R$, where the left-handed states form a $\mathrm{SU}(2)_L$ doublet with the soft SUSY breaking mass M_{3SQ}, and the right-handed states are $\mathrm{SU}(2)_L$ singlets with soft SUSY breaking masses $M_{3\mathrm{SU}}, M_{3\mathrm{SD}}$. For the sbottom sector, the mass matrix in the basis of $(\tilde{b}_L, \tilde{b}_R)$ is [4,5]

$$M_{\tilde{b}}^2 = \begin{pmatrix} M_{3SQ}^2 + m_b^2 + \Delta_{\tilde{d}_L} & m_b\tilde{A}_b \\ m_b\tilde{A}_b & M_{3\mathrm{SD}}^2 + m_b^2 + \Delta_{\tilde{d}_R} \end{pmatrix}, \quad (1)$$

where

$$\Delta_{\tilde{d}_L} = \left(-\frac{1}{2} + \frac{1}{3}\sin^2\theta_W\right)\cos 2\beta M_Z^2,$$
$$\Delta_{\tilde{d}_R} = \frac{1}{3}\sin^2\theta_W \cos 2\beta M_Z^2 \quad (2)$$

are the contributions from the $\mathrm{SU}(2)_L$ and $\mathrm{U}(1)_Y$ D-term quartic interactions. The trilinear soft SUSY breaking coupling A_b leads to the off-diagonal term $\tilde{A}_b = A_b - \mu\tan\beta$, which induces the mixing between left-handed and right-handed sbottom states. The lighter and heavier mass eigenvalues will be denoted as $m_{\tilde{b}_1}$ and $m_{\tilde{b}_2}$, respectively.

The left-handed mass parameter M_{3SQ} also controls the mass of the lighter stop. Since the stop sector provides the dominant contribution to the Higgs mass corrections, the naturalness argument prefers a relatively lower value of the stop mass. It is thus reasonable to consider $m_b\tilde{A}_b$, $M_{3SQ}^2 < M_{3\mathrm{SD}}^2$, and the lighter sbottom mass eigenstate is mostly left-handed $\tilde{b}_1 \sim \tilde{b}_L$. The left-handed sbottom couples to a bottom quark and a neutralino (or a top quark and a chargino) mainly through $\mathrm{SU}(2)_L$ gauge coupling and top Yukawa coupling, depending on the components of the neutralinos/charginos. Although the sbottom corrections to the Higgs mass are small compared to that from the

stop, there can be significant modification to the Higgs couplings, especially the bottom Yukawa coupling [6,20].

A right-handed sbottom $\tilde{b}_R$, on the other hand, couples to the $U(1)_Y$ gaugino and Higgsinos only via the hypercharge and Yukawa coupling. Its mass is determined by M^2_{3SD}. We will also consider the situation when it is light.

B. Sbottom decays

The most commonly studied channel in experimental searches is the case $\tilde{b}_1 \to b\chi^0_1$ with a branching fraction of 100%. This is true for the case with the Bino-LSP and the sbottom-NLSP, or the case with the stop-NLSP but $m_{\tilde{b}} < m_{\tilde{t}} + M_W$, or the case with the Wino-NLSP for a right-handed sbottom. In a more general ground, sbottom decays lead to a much richer pattern.

1. The decay of $\tilde{b}_L$

For a more general electroweakino spectrum, other decay channels may appear or even dominate, as analyzed in detail in Ref. [21]. We first consider the case of the lighter sbottom being mainly left-handed $\tilde{b}_1 \sim \tilde{b}_L$. The mass spectrum of sbottom and gaugino would influence severely the decay modes of sbottom. We discuss the (mainly left-handed) sbottom decay in details in the two general situations with a Bino-LSP,

$$m_{\tilde{b}_1} > M_2 > M_1 \quad (\text{Wino} - \text{NLSP}), \tag{3}$$

$$m_{\tilde{b}_1} > |\mu| > M_1 (\text{Higgsino} - \text{NLSP}). \tag{4}$$

The more involved cases when both Winos and Higgsinos are below the sbottom mass threshold

$$m_{\tilde{b}_1} > |\mu| > M_2 > M_1 \quad (\text{Wino} - \text{NLSP}/\text{Higgsino} - \text{NNLSP}), \tag{5}$$

$$m_{\tilde{b}_1} > M_2 > |\mu| > M_1 \quad (\text{Higgsino} - \text{NLSP}/\text{Wino} - \text{NNLSP}), \tag{6}$$

are also included when distinct features are present (sometimes referred as mixed NLSPs).

We illustrate the sbottom decay in Fig. 1 for these four different situations. Each corresponds to a different mass spectrum of gaugino and sbottom for a Bino-LSP. The usually considered channel $b\chi^0_1$ is suppressed, if other channels are open, since the bino $U(1)_Y$ coupling is smaller than the wino $SU(2)_L$ coupling or top Yukawa coupling. In Fig. 1(a), where $\tilde{b}_1 \to t\chi^\pm_1$ and $\tilde{b}_1 \to b\chi^0_2$ are open while the Higgsinos-like neutralinos/charginos are decoupling ($|\mu| > M_{\tilde{b}_1} > M_2 > M_1$), sbottom decays dominantly into $t\chi^\pm_1$ and $b\chi^0_2$. Contrarily, in Fig. 1(b), we decouple the Wino-like gaugino while leaving the channel containing the

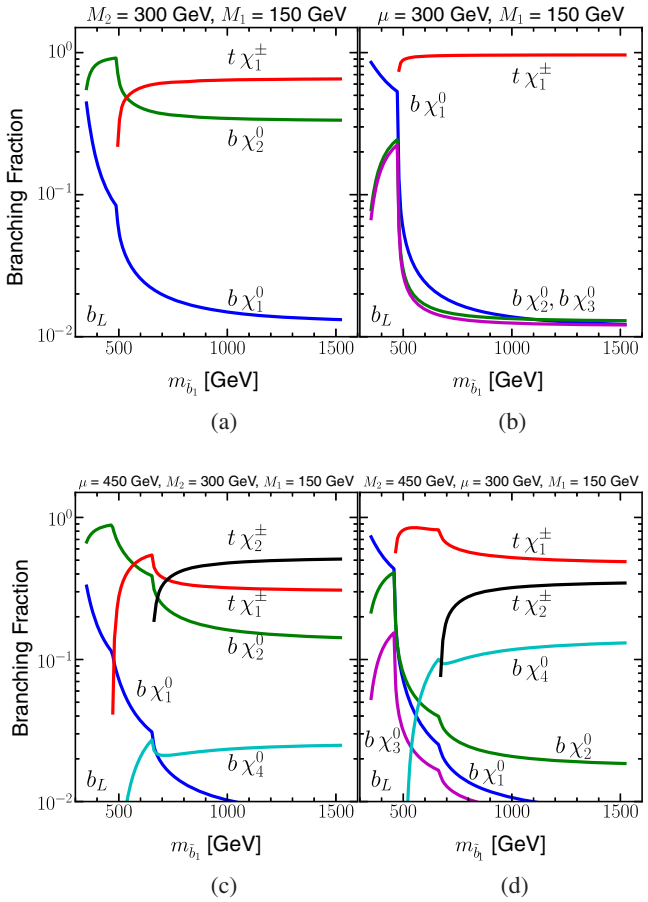

FIG. 1 (color online). Branch fractions of the left-handed sbottom decay versus its mass in four different cases: (a) $m_{\tilde{b}_1} > M_2 > M_1$, Wino-NLSP; (b) $m_{\tilde{b}_1} > |\mu| > M_1$, Higgsino-NLSP; (c) $m_{\tilde{b}_1} > |\mu| > M_2 > M_1$, Wino-NLSP/Higgsino-NNLSP, and (d) $m_{\tilde{b}_1} > M_2 > |\mu| > M_1$, Higgsino-NLSP/Wino-NNLSP. Here we have adopted $\tan\beta = 10$.

Higgsino-like gaugino opening ($M_2 > M_{\tilde{b}_1} > |\mu| > M_1$), and $\tilde{b}_1 \to t\chi^\pm_1$ will soon dominant over other possible channels when the phase space is open due to the large top Yukawa coupling. $\tilde{b}_1 \to b\chi^0_{2,3}$ are suppressed due to the relatively small bottom Yukawa coupling. Here we have adopted $\tan\beta = 10$. For a larger value of $\tan\beta$, $b\chi^0_2$, $b\chi^0_3$ channels will be relatively more important. For a more complicated situation, in the lower two panels, we consider the cases of $M_{\tilde{b}_1} > |\mu| > M_2 > M_1$ [Fig. 1(c)] and $M_{\tilde{b}_1} > M_2 > |\mu| > M_1$ [Fig. 1(d)]. In both cases, sbottom decays dominantly into a Higgsino-like chargino, then a Wino-like chargino, and at last a Wino-like neutralino. Other channels are highly suppressed since the $U(1)_Y$ coupling and bottom Yukawa coupling are much smaller.

A special remark is in order. Although $\tilde{b}_L$ and $\tilde{t}_L$ share the same soft mass parameter M_{3SQ}, the large mixing between $\tilde{t}_L - \tilde{t}_R$ due to the large trilinear soft SUSY breaking A_t often drags the mass of the (mixed) stop

below that of the (mainly left-handed) sbottom. The decay $\tilde{b}_1 \to W\tilde{t}_1$ usually dominates once it is kinematically open. However, the about decay patterns still hold as long as $M_{\tilde{b}_1} < M_{\tilde{t}_1} + m_W$.

2. The decay of $\tilde{b}_R$

For $\tilde{b}_R$, the usually considered channel $b\chi_1^0$ is the dominant mode. We present the branching fractions of $\tilde{b}_R$ in Fig. 2, for (a) the Wino-NLSP and (b) the Higgsino-NLSP. We see that the channel $\tilde{b}_1 \to b\chi_1^0$ in the Wino-NLSP scenario is almost 100%, since the right-handed squark has no $SU(2)_L$ coupling. However, this channel in the Higgsino-NLSP scenario presents a branching fraction about 40%–60%, followed by the channel of $\tilde{b}_1 \to t\chi_1^\pm$ about 20%–30%, that due to the coupling effects of the right-handed squark to Bino or Higgsino is $U(1)_Y$ and bottom Yukawa, respectively.

C. Current bounds from LHC

Searches for direct stop and sbottom pair production have been performed at both ATLAS and CMS, with about 5 fb^{-1} data at $\sqrt{s} = 7$ TeV and about 20 fb^{-1} data at $\sqrt{s} = 8$ TeV [7–9,15–19,22–32]. The current reach for the stop is slightly worse than that of the sbottom, which has been summarized in Ref. [21]. The current searches for the sbottom mainly focus on the decay channel $\tilde{b}_1 \to b\chi_1^0$ assuming 100% decay, and the sbottom mass up to 620 (700) GeV is excluded at 95% C.L. for a massless LSP with two b plus $\not{E}_T$ final states based on ATLAS (CMS) analyses [7,8]. For small mass splitting between sbottom and the LSP, $m_{\tilde{b}} - m_{\chi_1^0} \sim m_b$, the monojet plus $\not{E}_T$ search excludes a sbottom mass up to about 255 GeV [9].

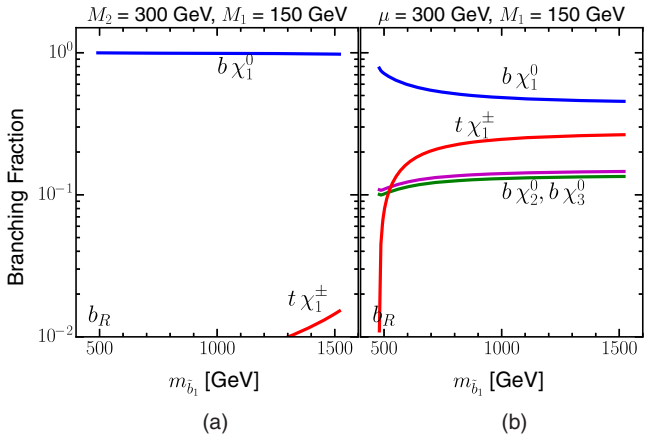

FIG. 2 (color online). Branch fractions of the right-handed sbottom decay versus its mass for (a) $m_{\tilde{b}_1} > M_2 > M_1$, Wino-NLSP, and (b) $m_{\tilde{b}_1} > |\mu| > M_1$, Higgsino-NLSP. Here we have adopted $\tan\beta = 10$.

Sbottom searches for $\tilde{b} \to b\chi_2^0$, $\chi_2^0 \to \chi_1^0 h$ with a 100% decay branching fraction have been performed at ATLAS [15], and the null search results exclude the sbottom masses between 340 and 600 GeV for $m_{\chi_2^0} = 300$ GeV and $m_{\chi_1^0} = 60$ GeV. For $\tilde{b} \to b\chi_2^0$, $\chi_2^0 \to \chi_1^0 Z$ with a 100% decay branching fraction, CMS searches exclude sbottom masses up to 450 GeV for LSP masses between 100 to 125 GeV and $m_{\chi_2^0} - m_{\chi_1^0} = 110$ GeV [16]. Sbottom searches for $\tilde{b} \to t\chi_1^\pm$, $\chi_1^\pm \to W\chi_1^0$ with a 100% decay branching fraction have been performed at both ATLAS and CMS [17,18]. The sbottom mass limit by ATLAS is about 440 GeV for $m_{\chi_1^\pm} < m_{\tilde{b}} - m_t$ [17], and the CMS limits for those channels are about 50 to 100 GeV stronger [16,18,19]. We summarize the current search bounds in Table I.

III. LHC ANALYSIS

In this section, we study the collider phenomenology of the light sbottom at the 14 TeV LHC. The key point in this paper is to explore the mixed decay channels according to the mass hierarchies beyond the common assumption of the 100% branching fraction of a given channel. Including those channels listed in Table I with realistic branching fractions would help increase the overall sensitivity, but we did not repeat the analyses. We note that Ref. [33] also exploited the mixed decays to search for stop. They introduced a new variable "topness" for the top-rich signal events to help efficiently reduce the top pair backgrounds.

A. Signature of $\tilde{b}_1 \sim \tilde{b}_L$

We consider the scenario with the low energy mass spectrum containing a light sbottom (mostly left-handed), a Bino-like LSP, and Wino-like NLSPs, as shown in Fig. 1(a). Two typical benchmark points for both signs of μ are listed in Table. II. Other soft SUSY breaking parameters are decoupled to be 2 TeV, and $\tilde{A}_t$ is set to be large such that the SM-like Higgs is around 125 GeV. The value of μ is chosen such that χ_2^0 dominantly decays to $h\chi_1^0$ for $\mu > 0$ and to $Z\chi_1^0$ for $\mu < 0$.[1] The decay channels and the corresponding decay branching fractions for $\tilde{b}_1$, $\tilde{t}_1$, as well as χ_2^0 and $\chi_1^\pm$, are listed in Table III. The conventional channel $\tilde{b}_1 \to b\chi_1^0$ is highly suppressed, with only about a 2% branching fraction, which dramatically weakens the current experimental search limit. The decay channels of $\tilde{b}_1 \to b\chi_2^0$ and $\tilde{b}_1 \to t\chi_1^-$ are comparable and dominant instead. In particular, with one sbottom decaying to χ_2^0 and one sbottom decaying to $\chi_1^\pm$, $\tilde{b}_1\tilde{b}_1^*$ pair production leads to interesting final states of $bbWW + h/Z + \not{E}_T$. Note that

[1]Note that $\chi_2^0 \to Z\chi_1^0$ is not always dominated for $\mu < 0$, as pointed out in Refs. [34,35]. We have chosen the value of μ in the $\mu < 0$ case to guarantee the Z channel dominance.

TABLE I. Current mass bounds on the sbottom from the direct searches at the LHC.

Decay channels	Mass bounds $m_{\tilde{b}}$	Branching ratio	Assumptions
$\tilde{b}_1 \to b\chi_1^0$ (ATLAS [8])	620 GeV	100%	$m_{\chi_1^0} < 120$ GeV
	520 GeV	60%	$m_{\chi_1^0} < 150$ GeV
$\tilde{b}_1 \to b\chi_1^0$ (ATLAS [9])	255 GeV	100%	$m_{\tilde{b}} - m_{\chi_1^0} \sim m_b$
$\tilde{b}_1 \to b\chi_1^0$ (CMS [7])	700 GeV	100%	Small $m_{\chi_1^0}$
$\tilde{b}_1 \to b\chi_2^0 \to bh\chi_1^0$ (ATLAS [15])	340–600 GeV	100%	$m_{\chi_2^0} = 300$ GeV
			$m_{\chi_1^0} = 60$ GeV
$\tilde{b}_1 \to b\chi_2^0 \to bZ\chi_1^0$ (CMS [16])	450 GeV	100%	100 GeV $< m_{\chi_1^0} <$ 125 GeV
			$m_{\chi_2^0} - m_{\chi_1^0} = 110$ GeV
$\tilde{b}_1 \to t\chi_1^-$ (ATLAS [17])	440 GeV	100%	$m_{\chi_1^\pm} < m_{\tilde{b}} - m_t$
	575 GeV	100%	150 GeV $< m_{\chi_1^\pm} <$ 375 GeV
			$m_{\chi_1^0} = 50$ GeV
$\tilde{b}_1 \to t\chi_1^-$ (CMS [16])	575 GeV	100%	25 GeV $< m_{\chi_1^0} <$ 150 GeV
			$\frac{m_{\chi_1^0}}{m_{\chi_1^\pm}} = 0.5$
	525 GeV	100%	25 GeV $< m_{\chi_1^0} <$ 200 GeV
			$\frac{m_{\chi_1^0}}{m_{\chi_1^\pm}} = 0.8$
$\tilde{b}_1 \to t\chi_1^-$ (CMS [18])	500 GeV	100%	$\frac{m_{\chi_1^0}}{m_{\chi_1^\pm}} = 0.5$ (0.8)
$\tilde{b}_1 \to t\chi_1^-$ (CMS [19])	550 GeV	100%	$m_{\chi_1^0} = 50$ GeV

TABLE II. MSSM parameters and the mass spectrum of SUSY particles for the two benchmark points. All masses are in units of GeV.

	M_1	M_2	M_{3SQ}	A_t	μ	$\tan\beta$	$m_{\chi_1^0}$	$m_{\chi_2^0}$	$m_{\chi_1^\pm}$	$m_{\tilde{b}_1}$	$m_{\tilde{t}_1}$	m_h
BP1	150	300	650	2950	+2000	10	152	320	320	640	650	125
BP2	150	300	650	2950	−1300	10	150	320	320	640	630	125

unmixed decays of $\tilde{b}_1\tilde{b}_1^* \to bbhh + \not{E}_T$, $bbZZ + \not{E}_T$, $ttWW + \not{E}_T$ have been studied at the LHC [15–19], assuming a 100% decay branching fractions. Given the more realistic branching fractions of about 40% for $\tilde{b}_1 \to b\chi_2^0$ and about 60% for $\tilde{b}_1 \to t\chi_1^-$, the collider limits for those channels will be relaxed. Including all the mixed and unmixed channels can further increase the collider reach for the sbottom.

The stop decay has been studied in detail in Ref. [21]. For the two benchmark points listed in Table II, the conventional decay channel $\tilde{t}_1 \to t\chi_1^0$ is highly suppressed. $\tilde{t}_1 \to b\chi_1^-$ is dominant with a branching fraction of about 70%. $\tilde{t}_1 \to t\chi_2^0$ is subdominant with a branching fraction of about 27%. With one stop decaying to χ_2^0 and one stop decaying to χ_1^0, $\tilde{t}_1\tilde{t}_1^*$ pair production provides the same final states as the sbottom case.

TABLE III. Decay channels and the corresponding branching fractions of $\tilde{b}_1$, $\tilde{t}_1$, χ_2^0, and χ_1^+ for the two benchmark points, which correspond to the cases of $\mu > 0$ and $\mu < 0$.

	Decay channel	Branching ratio	Decay channel	Branching ratio	Decay channel	Branching ratio
BP1 ($\mu > 0$)	$\tilde{b}_1 \to b\chi_1^0$	2%	$\tilde{t}_1 \to t\chi_1^0$	2%	$\chi_2^0 \to h\chi_1^0$	97%
	$\tilde{b}_1 \to b\chi_2^0$	39%	$\tilde{t}_1 \to t\chi_2^0$	27%	$\chi_2^0 \to Z\chi_1^0$	3%
	$\tilde{b}_1 \to t\chi_1^-$	59%	$\tilde{t}_1 \to b\chi_1^+$	71%	$\chi_1^\pm \to W^\pm\chi_1^0$	100%
BP2 ($\mu < 0$)	$\tilde{b}_1 \to b\chi_1^0$	2%	$\tilde{t}_1 \to t\chi_1^0$	2%	$\chi_2^0 \to h\chi_1^0$	6%
	$\tilde{b}_1 \to b\chi_2^0$	39%	$\tilde{t}_1 \to t\chi_2^0$	27%	$\chi_2^0 \to Z\chi_1^0$	94%
	$\tilde{b}_1 \to t\chi_1^-$	59%	$\tilde{t}_1 \to b\chi_1^+$	71%	$\chi_1^\pm \to W^\pm\chi_1^0$	100%

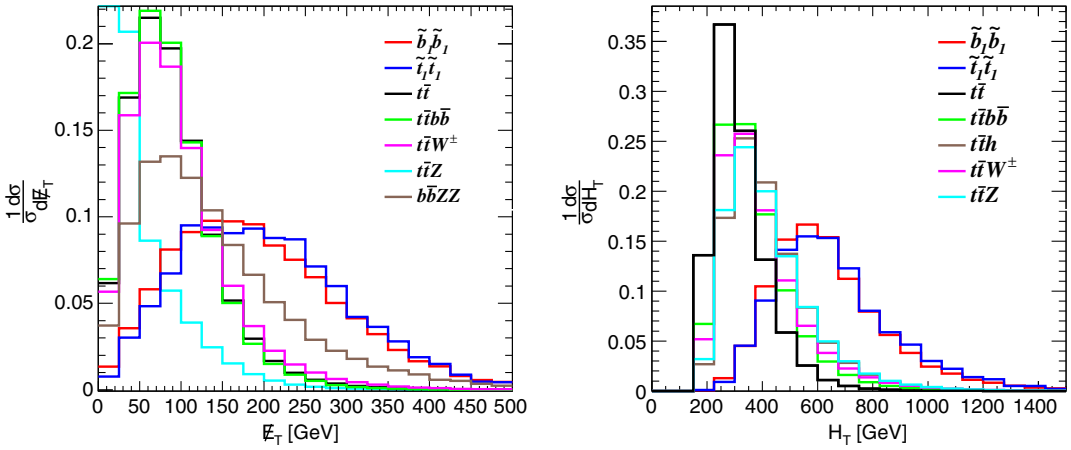

FIG. 3 (color online). Normalized distributions of $\not{E}_T$ (left panel) and H_T (right panel) for the signal $\tilde{b}_1\tilde{b}_1^*$ (red curves), $\tilde{t}_1\tilde{t}_1^*$ (blue curves) $\to bbWWh\not{E}_T \to \ell bbbbjj\not{E}_T$ after basic cuts with $m_{\tilde{b}_1} = 637$ GeV, $m_{\tilde{t}_1} = 646$ GeV, as well as SM backgrounds at the 14 TeV LHC.

The two benchmark points listed in Table II are only for illustration whenever instructive. In our following analyses, we perform a broad scan over the mass parameter space:

(i) M_{3SQ} from 400 to 1075 GeV with a step size of 25 GeV, corresponding to $m_{\tilde{b}_1}$ from about 350 GeV to about 1085 GeV and $m_{\tilde{t}_1}$ from about 367 GeV to about 1090 GeV.
(ii) M_1 is scanned from 3 GeV to 700 GeV, in the step of 25 GeV.
(iii) M_2 is fixed to be $M_2 = M_1 + 150$ GeV.
(iv) We further require $m_{\tilde{b}_1} > m_{\chi_1^\pm} + m_t$ such that $\tilde{b}_1 \to t\chi_1^\pm$ can be open.

In our phenomenological studies, we define the basic observable objects as

(i) Jet:

$$|\eta_j| < 2.5, \quad p_T^j > 25\,\text{GeV}, \quad \Delta\phi_{j,\not{E}_T} > 0.8, \quad (7)$$

where $\Delta\phi_{j,\not{E}_T}$ is the azimuthal angle between the jet and missing transverse energy.

(ii) Lepton:

$$|\eta_\ell| < 2.5, \quad p_T^\ell > 20\,\text{GeV}, \quad \Delta R_{\ell j} > 0.4, \quad (8)$$

where $\Delta R_{\ell j}$ is the distance in the ϕ-η plane $\Delta R = \sqrt{\Delta\phi^2 + \Delta\eta^2}$, between the lepton and the jet satisfying Eq. (7).

To be as realistic as possible, both the signal and the background samples are generated by MadGraph 5[36], passed through PYTHIA 6[37] for the fragmentation and hadronization. We further perform the detector simulation through Delphes 3 [38] with Snowmass Delphes No-Pile-up detector cards [39].

1. The Case of $\mu > 0$: Final states with a Higgs

In the case of $\mu > 0$, the leading signal under consideration for the pair production of the sbottom, with $\tilde{b}_1 \to b\chi_2^0 \to bh\chi_1^0$ and $\tilde{b}_1^* \to t\chi_1^- \to bW^+W^-\chi_1^0$, is

$$\tilde{b}_1\tilde{b}_1^* \to bbWWh\not{E}_T \to \ell bbbbjj\not{E}_T.$$

The signal contains four b-jets, two light flavor jets, one isolated lepton (e or μ), and a large missing energy. The study of the same final state from the stop decay can be found in Ref. [21]. The dominant backgrounds will be from $t\bar{t}$ + jets and $t\bar{t}b\bar{b}$ with large cross sections and similar final states. While $t\bar{t}h$ is an irreducible background, the production cross section is relatively small. Other SM backgrounds include $t\bar{t}W$, $t\bar{t}Z$, and $b\bar{b}WW$, with typically smaller cross sections.

To select the signal of $\tilde{b}_1\tilde{b}_1^*$, $\tilde{t}_1\tilde{t}_1^* \to bbWWh\not{E}_T \to \ell bbbbjj\not{E}_T$, we adopt the basic event selection:

(i) $N_j \geq 4$, $p_T^{j1,j2,j3} > 40$ GeV, $N_\ell = 1$.

Beside these basic cuts, we further optimize the cuts and divide the events into signal regions on the following variables:

(i) Missing energy $\not{E}_T$, which is the magnitude of the the missing transverse momentum, to be above 100, 120, 140, 160 180, and 200 GeV.
(ii) H_T, the scalar sum of the jet transverse momentum of all surviving isolated jets: $H_T = \sum_{\text{jets}} |p_T^j|$, to be above 400, 450, 500, 550, 600 GeV.
(iii) M_T, the transverse mass, defined as the invariant mass of the lepton and missing energy,

$$M_T(\mathbf{p}_T^\ell, \mathbf{p}_T^{\text{miss}}) = \sqrt{2p_T^\ell p_T^{\text{miss}}(1 - \cos\phi_{\ell,\not{E}_T})}, \quad (9)$$

to be above 100, 120, 140, 160, 180, 200 GeV.

TABLE IV. Cut efficiencies and cross sections before and after cuts for the signal $\tilde{b}_1\tilde{b}_1^*, \tilde{t}_1\tilde{t}_1^* \to bbWWh\not{E}_T \to \ell bbbbjj\not{E}_T$ for BP1 listed in Table II for $\mu > 0$, as well as SM backgrounds at the 14 TeV LHC. The significance is obtained for $\int Ldt = 300$ fb^{-1} with a 10% systematic error combining both sbottom and stop signals.

Process	σ [fb]	Basic cuts	$\not{E}_T > 200$ GeV	$H_T > 500$ GeV	$M_T > 160$ GeV	$N_j \geq 5$	$N_b \geq 2$	σ [fb] after cuts
$\tilde{b}_1\tilde{b}_1$	13	39%	17%	14%	5.8%	4.3%	2.7%	3.4×10^{-1}
$\tilde{t}_1\tilde{t}_1$	10	39%	18%	16%	5.9%	4.4%	2.9%	2.9×10^{-1}
$t\bar{t}$	260,000	14%	0.24%	7.4×10^{-4}	1.7×10^{-6}	9.3×10^{-7}	2.4×10^{-7}	6.3×10^{-2}
$t\bar{t}b\bar{b}$	2,300	24%	0.6%	0.3%	3.5×10^{-5}	2.3×10^{-5}	1.2×10^{-5}	2.8×10^{-2}
$t\bar{t}h$	100	31%	1.2%	0.8%	5.8×10^{-5}	3.4×10^{-5}	1.9×10^{-5}	2.0×10^{-3}
$t\bar{t}Z$	230	30%	1.2%	0.8%	6.6×10^{-5}	3.9×10^{-5}	9.8×10^{-6}	2.2×10^{-3}
$t\bar{t}W^{\pm}$	224	25%	1.2%	0.7%	4.8×10^{-5}	2.3×10^{-5}	6.3×10^{-6}	1.4×10^{-3}
				$\sqrt{s} = 14$ TeV $\int Ldt = 300$ fb^{-1}				
				$\frac{S}{\sqrt{B+(10\%B)^2}} = 17$ (14) for $\tilde{b}_1$ ($\tilde{t}_1$)				

(iv) N_j, the multiplicity of all surviving isolated jets, being at least 4, 5, and 6.

(v) N_b, the multiplicity of tagged b-jets, being at least 2, 3, and 4.

The normalized distributions of $\not{E}_T$ and H_T are shown in Fig. 3. As expected, the signal process has larger $\not{E}_T$ from the missing neutralino-LSP than the background processes, which is typically bounded by $m_W/2$ due to the primary contribution $W \to \ell\nu$. Given the relatively large sbottom mass, the signal process typically has larger H_T than the SM backgrounds as well.

In Table IV, we list the cumulative cut efficiencies after different levels of cuts, as well as cross sections before and after cuts for both the sbottom and the stop signals as well as the SM backgrounds for the benchmark point listed in Table II for $\mu > 0$. The cross section for each process is normalized to their theoretical values including next leading order QCD corrections [40–46]. The background processes are significantly suppressed after strong $\not{E}_T$, H_T, M_T cuts. The leading background left is $t\bar{t}$, followed by $t\bar{t}b\bar{b}$. We scan over the combinations of the signal regions, to select the optimal combination which gives the best significance for each mass grid point, including 10% systematic uncertainty. At $\sqrt{s} = 14$ TeV with 300 fb^{-1} integrated luminosity, the significance could reach about 17σ (14σ) for $\tilde{b}_1$ ($\tilde{t}_1$) of about 640 GeV.

Signal significance contours are shown in Fig. 4 with the 5σ discovery reach (black curve) and 95% C.L. exclusion limit (red curve) for 14 TeV LHC with 300 fb^{-1} integrated luminosity. Figure 4(a) shows the $m_{\tilde{b}_1}$-$m_{\chi_1^0}$ plane. We find that the 5σ discovery can reach about 750 GeV for $\tilde{b}_1$ when χ_1^0 is almost massless and reach about 920 GeV when χ_1^0 is about 200 GeV to 300 GeV. The 95% C.L. exclusion reach is about 100 GeV better. The reach for the stop with the same final states can be found in Ref. [21], with results being very similar.

Since the (mostly left-handed) sbottom and stop have the same undistinguishable final states with their masses controlled by the same parameter M_{3SQ}, we present the combined reach of stop and sbottom in Fig. 4(b) in M_{3SQ}-$m_{\chi_1^0}$ plane.[2] The 5σ discovery reach in M_{3SQ} increases to be 820 GeV for a massless LSP, and 1080 GeV for $m_{\chi_1^0} \sim 300$ GeV. The masses up to 980 GeV can be excluded for a massless LSP, and the masses up to 1180 GeV can be excluded for $m_{\chi_1^0} \sim 300$ GeV at 95% C.L.

We would like to reiterate that the mixing in sbottom and stop sectors governs the mass spectrum of the sbottom and stop. Small mixing in the sbottom sector is always a good approximation given the small bottom Yukawa coupling, while the mixing in the stop sector may be large enough to suppress the mass of the lighter stop further. In our cases (including the $\mu < 0$ case discussed below), the right-handed stop is assumed to be very heavy (decoupled to be 2 TeV), which will result in a smaller mixing for a large range of $A_t \in [-4000, 4000]$ GeV. Furthermore, even if a large mixing in the stop sector gives a much lighter stop compared with the sbottom, this would potentially lead to a better signal in the stop sector. The combination of the stop and sbottom signals, however, does not depend on the mass difference between the stop and sbottom. In the parameter space that we are considering with relatively small stop and sbottom mass difference, both channels contribute significantly to the combined reach. In cases when the mass difference between the stop and sbottom is large, only one channel will contribute dominantly to the combined significance.

2. The case of $\mu < 0$: Final states with a Z-boson

For the case of $\mu < 0$, the dominant decay channel of χ_2^0 is $\chi_2^0 \to Z\chi_1^0$ instead [47]. The leading signal under consideration for the pair production of sbottom and stop with

[2]The mass difference between the stop and sbottom does not affect the combination of the stop and sbottom signals, since the same cuts are used for both the stop and the sbottom events.

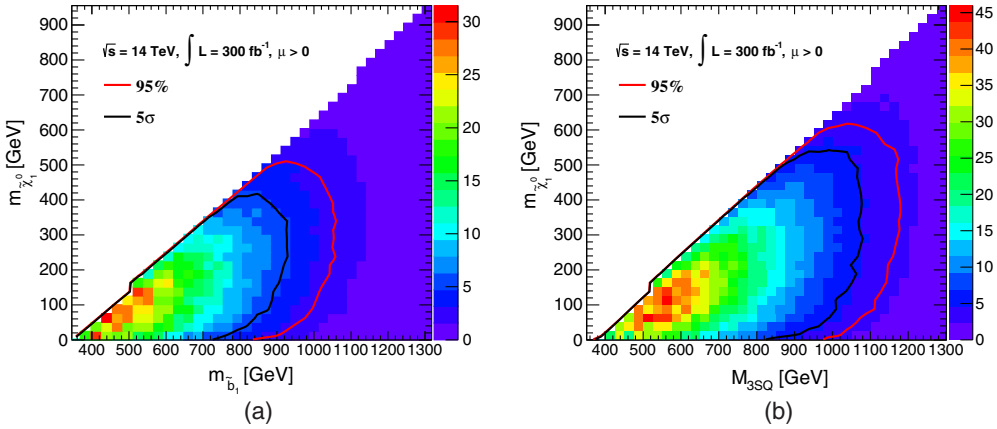

FIG. 4 (color online). Signal significance contours for $\tilde{b}_1\tilde{b}^*$, $\tilde{t}_1\tilde{t}_1^* \to bbWWh\not{E}_T \to \ell bbbbjj\not{E}_T$ final states for 14 TeV LHC with $\int Ldt = 300$ fb^{-1} luminosity. The 5σ discovery reach (black curves) and 95% C.L. exclusion limit (red curves) for the sbottom only are shown in the (a) $m_{\tilde{b}_1}$-$m_{\chi_1^0}$ plane, and in the (b) M_{3SQ}-$m_{\chi_1^0}$ plane for the combined reach for sbottom and stop.

$\tilde{b}_1 \to b\chi_2^0 \to bZ\chi_1^0$, $\tilde{b}_1^* \to t\chi_1^- \to bW^+W^-\chi_1^0$ and $\tilde{t}_1 \to t\chi_2^0 \to bW^+Z\chi_1^0$, $\tilde{t}_1^* \to b\chi_1^- \to bW^-\chi_1^0$ is then

$$\tilde{b}_1\tilde{b}_1^*, \qquad \tilde{t}_1\tilde{t}_1^* \to bbWWZ\not{E}_T \to \ell^+\ell^- bbjjjj\not{E}_T.$$

The signal contains two b-jets, four light flavor jets, two same flavor, opposite sign leptons, and large missing energy. The two leptons are used to reconstruct the Z boson, which will significantly reduce the SM backgrounds. The dominant background is $t\bar{t}$ plus one or two additional QCD jets.

We impose the basic event selection cuts as the previous case. We again optimize the cuts and divide the events into signal regions:

(i) $\not{E}_T$ to be above 100, 120, 140, 160 180, and 200 GeV.
(ii) H_T to be above 400, 450, 500, 550, 600 GeV.
(iii) M_{T2}, the lepton-bashed transverse mass [48–50]

$$M_{T2}(\mathbf{p}_T^{\ell_1}, \mathbf{p}_T^{\ell_2}, \mathbf{p}_T^{\rm miss}) = \min_{\mathbf{p}_{T,1}^{\rm miss}+\mathbf{p}_{T,2}^{\rm miss}=\mathbf{p}_T^{\rm miss}} \{\max\{M_T(\mathbf{p}_T^{\ell_1}, \mathbf{p}_{T,1}^{\rm miss}), M_T(\mathbf{p}_T^{\ell_2}, \mathbf{p}_{T,2}^{\rm miss})\}\} \tag{10}$$

to be above 75, 80, 85, 90 GeV.
(iv) $\Delta M_{\ell\ell} = |M_{\ell\ell} - m_Z|$, being less than 10 GeV.
(v) N_j being at least 4, 5, and 6.
(vi) N_b being at least 1 to suppress the enormous QCD backgrounds with light flavor jets.

The normalized distributions of $\not{E}_T$ and M_{T2} for both the sbottom and the stop signals, as well as the SM backgrounds, are presented in Fig. 5. The $\not{E}_T$ distributions for the signal typically extend to larger values. The $M_{T2}(\mathbf{p}_T^{\ell_1}, \mathbf{p}_T^{\ell_2}, \mathbf{p}_T^{\rm miss})$ distributions for SM backgrounds with

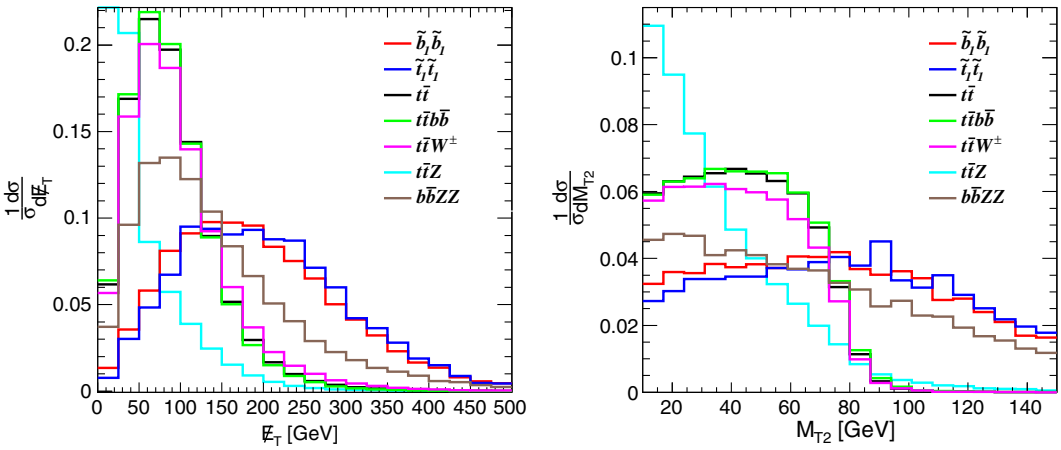

FIG. 5 (color online). Normalized distributions $\not{E}_T$ (left panel) and M_{T2} (right panel) for the signal $\tilde{b}_1\tilde{b}^*$ (red curves), $\tilde{t}_1\tilde{t}_1^*$ (blue curves) $\to bbWWZ\not{E}_T \to \ell^+\ell^- bbjjjj\not{E}_T$ after basic cuts with $m_{\tilde{b}_1} = 637$ GeV, $m_{\tilde{t}_1} = 634$ GeV, as well as SM backgrounds at the 14 TeV LHC.

TABLE V. Cut efficiencies and cross sections before and after cuts for the signal $\tilde{b}_1\tilde{b}_1^*, \tilde{t}_1\tilde{t}_1^* \to bbWWZ\not{E}_T \to \ell^+\ell^- bbjjjj\not{E}_T$, for BP2 in Table II for $\mu < 0$, as well as dominant SM backgrounds at the 14 TeV LHC. The significance is obtained for $\int Ldt = 300\text{fb}^{-1}$ with 10% systematic error combining both sbottom and stop signals.

Process	σ [fb]	Basic cuts	$\not{E}_T > 175$ GeV	$H_T > 400$ GeV	$M_{T2} > 90$ GeV	$\Delta M_{ll} < 10$ GeV	$N_j \geq 4$	$N_b \geq 1$	σ [fb] after cuts
$\tilde{b}_1\tilde{b}_1$	2.1	32%	17%	16%	5.8%	5.3%	5.3%	4.2%	8.8×10^{-2}
$\tilde{t}_1\tilde{t}_1$	1.8	27%	16%	11.2%	4.9%	4.4%	4.4%	3.6%	6.5×10^{-2}
$t\bar{t}$	33,000	1.3%	0.09%	0.06%	5.0×10^{-6}	4.9×10^{-7}	4.9×10^{-7}	3.7×10^{-7}	1.2×10^{-2}
$t\bar{t}Z$	71	11%	0.25%	0.16%	5.8×10^{-5}	4.2×10^{-5}	4.2×10^{-5}	2.7×10^{-5}	1.9×10^{-3}
$t\bar{t}b\bar{b}$	400	3.2%	0.20%	0.12%	1.4×10^{-5}	2.0×10^{-6}	2.0×10^{-6}	1.8×10^{-6}	6.9×10^{-4}
$t\bar{t}ZZ$	0.16	16%	0.86%	0.64%	0.31%	0.27%	0.27%	0.18%	3.0×10^{-4}
$b\bar{b}ZZ$	2.3	0.39%	0.11%	0.06%	2.9×10^{-4}	2.6×10^{-4}	2.6×10^{-4}	2.1×10^{-4}	4.8×10^{-4}
				$\sqrt{s} = 14$ TeV $\int Ldt = 300$ fb^{-1}					
				$\frac{S}{\sqrt{B+(10\%B)^2}} = 12$ (8.7) for $\tilde{b}_1$ ($\tilde{t}_1$)					

the lepton pair coming from leptonic W decay are cut off at m_W, while the signal as well as the $bbZZ$ background have much flatter M_{T2} distributions. Note that while the distribution of the $bbZZ$ background is similar to that of the signal, the overall cross section for $bbZZ$ is negligibly small.

Another interesting variable for the sbottom case is $M_{\ell\ell b}$, which is related to $m_{\tilde{b}_1}$ if the b jet and the lepton pair from the same sbottom cascade decay chain $\tilde{b}_1 \to b\chi_2^0 \to bZ\chi_1^0$ can be identified. While we will not use it for event selection in our analyses, $M_{\ell\ell b}$ distribution could provide information on $m_{\tilde{b}_1}$ as well as $m_{\chi_2^0}$ if a sbottom signal is discovered.

The advanced cuts and the corresponding cumulative cut efficiencies as well as the cross sections for sbottom and

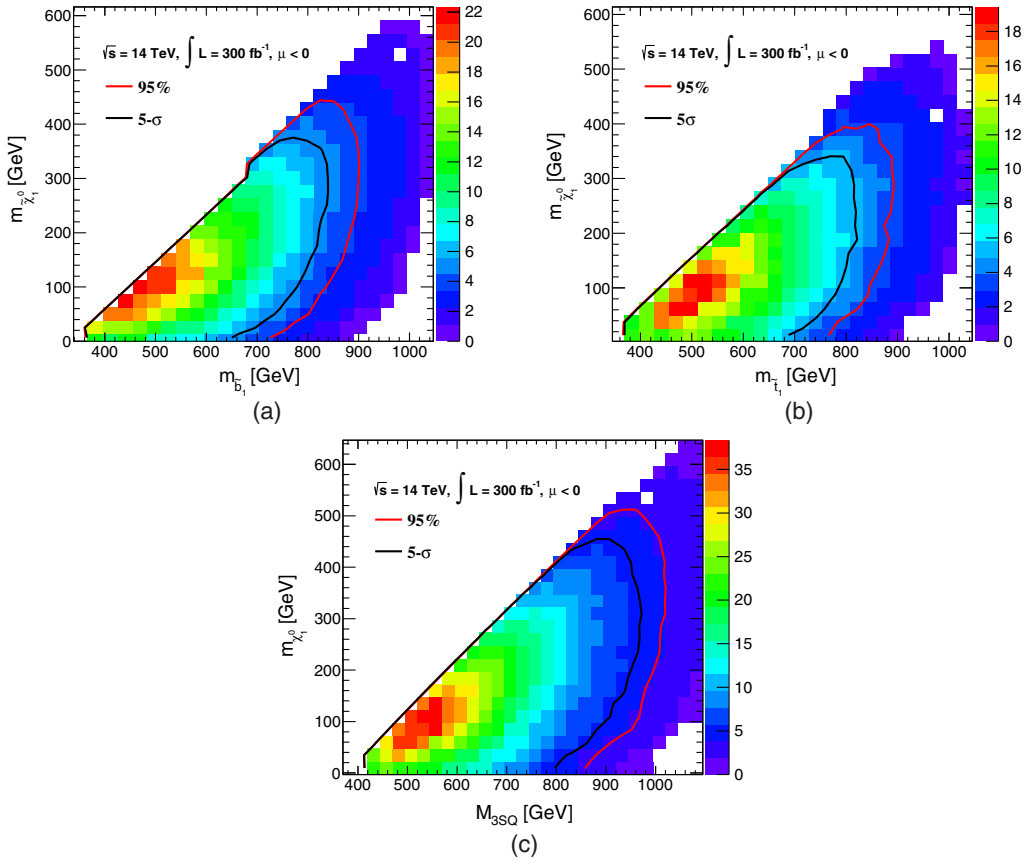

FIG. 6 (color online). Signal significance contours for $\tilde{b}_1\tilde{b}^*, \tilde{t}_1\tilde{t}_1^* \to bbWWZ\not{E}_T \to \ell^+\ell^- bbjjjj\not{E}_T$ final states for 14 TeV LHC with $\int Ldt = 300$ fb^{-1} luminosity. The 5σ discovery reach (black curves) and 95% C.L. exclusion limit (red curves) are shown in the (a) $m_{\tilde{b}_1}$-$m_{\chi_1^0}$ plane, in the (b) $m_{\tilde{t}_1}$-$m_{\chi_1^0}$ plane, and the combined reach in the (c) M_{3SQ}-$m_{\chi_1^0}$ plane.

TABLE VI. MSSM parameters and mass spectrum of SUSY particles for the benchmark point in the case of the right-handed sbottom. All masses are in units of GeV.

	M_1	M_2	M_{3SD}	A_t	μ	$\tan\beta$	$m_{\chi_1^0}$	$m_{\chi_1^\pm}$	$m_{\tilde{b}_1}$	m_h
BP3	150	2000	650	2895	300	10	145	307	635	125

TABLE VII. Decay channels and the corresponding branching fractions of $\tilde{b}_1$ and $\chi_1^\pm$ for the benchmark point, which corresponds to the case of the right-handed sbottom.

	Decay channel	Branching ratio	Decay channel	Branching ratio
BP3	$\tilde{b}_1 \to b\chi_1^0$	58%	$\chi_1^\pm \to \chi_1^0 W^\pm$	100%
	$\tilde{b}_1 \to t\chi_1^-$	18%		

stop signals for BP2 with $\mu < 0$ and SM backgrounds before and after cuts are given in Table V. The dominant SM background is $t\bar{t}$ plus jets. A significance of about 12σ (8.7σ) can be reached for $\tilde{b}_1$ ($\tilde{t}_1$) for the benchmark point at the 14 TeV LHC with 300 fb^{-1} luminosity, including 10% systematic error.

Signal significance contours are shown in Fig. 6 with the 5σ discovery reach (black curves) and 95% C.L. exclusion limit (red curves) for 14 TeV LHC with 300 fb^{-1} integrated luminosity, in the (a) $m_{\tilde{b}_1}$-$m_{\chi_1^0}$ plane, (b) $m_{\tilde{t}_1}$-$m_{\chi_1^0}$ plane, and (c) M_{3SQ}-$m_{\chi_1^0}$ plane. For massless χ_1^0, sbottom (stop) masses up to 650 (680) GeV can be discovered and 720 (760) will be excluded at 95% C.L. if there is no signal over SM backgrounds being found. For moderate mass of χ_1^0 around 200–300 GeV, the 5σ discovery can reach up to 820 (840) GeV, and the 95% exclusion limit can go up to 890 (900) GeV for sbottom (stop). The combined reach of the stop and sbottom is shown in Fig. 6(c) in the M_{3SQ} versus $m_{\chi_1^0}$ plane. About 980 GeV can be achieved in M_{3SQ} for the 5σ discovery reach and about 1025 GeV for the 95% C.L. exclusion. The experimental reach for the case of $\mu < 0$ is lower than that for the case of $\mu > 0$.

B. Signature of $\tilde{b}_1 \sim \tilde{b}_R$

To complete our exploration for the sbottom signal, we consider another scenario with the low energy mass spectrum containing a light mostly right-handed sbottom, a Bino-like LSP and Higgsino-like NLSPs. Here, the sign of μ does not affect the decay modes of sbottom and neutralinos. The typical benchmark point is listed in Table VI, and the corresponding branching fractions are listed in Table VII. Other soft SUSY breaking parameters are decoupled by setting them to be at 2 TeV. In this scenario, the right-handed sbottom couples to the Bino and Higgsino through the $U(1)_Y$ or the bottom Yukawa couplings, which results in the sbottom dominantly decaying to $b\chi_1^0$ due to the large phase space, followed by the channel $t\chi_1^\pm$ when it is kinematically open. We will focus on the signal reach of the sbottom pair production

$$\tilde{b}_1\tilde{b}_1^* \to b\chi_1^0 t\chi_1^\pm \to b\chi_1^0 tW^\pm\chi_1^0 \to \ell bbjj\not{E}_T.$$

The SM backgrounds are somewhat similar to that of the $\mu > 0$ case of the left-handed sbottom with fewer jets. We also include vector bosons plus additional jets as another background [51].

We scan over a broad mass parameter space: M_1 from 3 GeV to 800 GeV in steps of 30 GeV, M_{3SD} from 400 GeV to 1180 GeV in steps of 30 GeV; μ is fixed to be $\mu = M_1 + 150$ GeV. We further require that $m_{\tilde{b}_1} > m_{\chi_1^\pm} + m_t$ so that the decay channel $\tilde{b}_1 \to t\chi_1^\pm$ is kinematically accessible. Since the final state particles are stiffer than the previous cases with cascade decays, we apply stronger basic cuts than before. The basic event selection cuts are the following:

(i) Jet:

$$|\eta_j| < 2.5, \quad p_T^j > 40\ \text{GeV}, \quad \Delta\phi_{j,\not{E}_T} > 0.8. \quad (11)$$

(ii) Lepton:

$$|\eta_\ell| < 2.5, \quad p_T^\ell > 30\ \text{GeV}, \quad \Delta R_{\ell j} > 0.4. \quad (12)$$

TABLE VIII. Cut efficiencies and cross sections before and after cuts for the signal $\tilde{b}_1\tilde{b}_1^* \to bbWW\not{E}_T \to \ell bbjj\not{E}_T$, for BP3 in Table VI, as well as SM backgrounds at the 14 TeV LHC. The significance is obtained for $\int Ldt = 300$ fb^{-1} with 10% systematic error.

Process	σ [fb]	Basic cuts	$\not{E}_T > 200$ GeV	$H_T > 500$ GeV	$M_T > 160$ GeV	$N_j \geq 4$	$N_b \geq 1$	σ [fb] after cuts
$\tilde{b}_1\tilde{b}_1$	9.7	30%	20%	14%	8.1%	5.6%	5.6%	5.4×10^{-1}
$t\bar{t}$	260 000	5.3%	0.14%	4.7×10^{-4}	1.6×10^{-6}	8.1×10^{-7}	8.1×10^{-7}	2.1×10^{-1}
$t\bar{t}b\bar{b}$	2 300	13%	0.4%	0.2%	3.7×10^{-5}	2.6×10^{-5}	2.6×10^{-5}	6.1×10^{-2}
$t\bar{t}h$	100	20%	1%	0.7%	7.8×10^{-5}	5.2×10^{-5}	5.2×10^{-5}	5.3×10^{-3}
$t\bar{t}Z$	230	14%	0.7%	0.5%	8.1×10^{-5}	4.5×10^{-5}	4.5×10^{-5}	1×10^{-2}
$t\bar{t}W^\pm$	224	11%	0.7%	0.5%	6.6×10^{-5}	3.4×10^{-5}	3.4×10^{-5}	7.6×10^{-3}
Vjj	3.7×10^7	4.8×10^{-5}	2.9×10^{-6}	1.8×10^{-6}	2.9×10^{-9}	1×10^{-9}	1×10^{-9}	3.8×10^{-2}
			$\sqrt{s} = 14$ TeV $L = 300$ fb^{-1} $S/\sqrt{B + (10\%B)^2}$					11.4

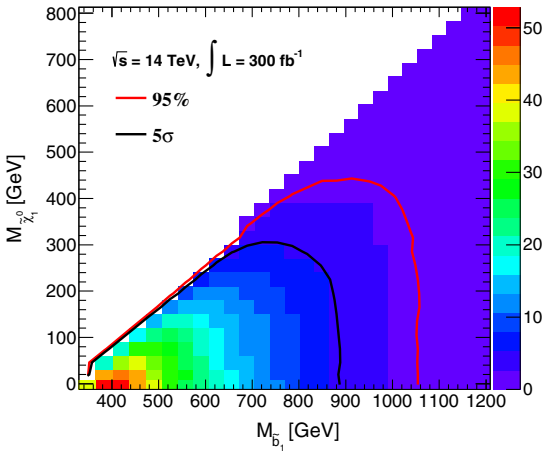

FIG. 7 (color online). Signal significance contours for $\tilde{b}_1\tilde{b}_1^* \to bbWW\not{E}_T \to \ell^\pm bbjj\not{E}_T$ final state for the right-handed sbottom in the $m_{\tilde{b}_1}$-$m_{\chi_1^0}$ plane for 14 TeV LHC with $\int Ldt = 300$ fb^{-1} luminosity. The 5σ discovery reach (black curve) and 95% C.L. exclusion limit (red curve) are shown.

(iii) At least three jets satisfying requirement Eq. (11), within which at least one is b-tagged, and exactly one lepton satisfying requirement Eq. (12).

(iv) The leading b-jet p_T is required to be larger than 100 GeV since one b-jet originates directly from a heavy sbottom decay.

Besides the basic event selection cuts, we apply the same advanced event selection cuts in the signal regions (H_T, $\not{E}_T$, M_T, N_j, and N_b) as in Sec. III A and optimize them for different mass parameters. In Table VIII, we list the cross section before and after the above cuts and also the efficiency after every cut for the benchmark point listed in Table VI.

Signal significance contours are shown in Fig. 7 with the 5σ discovery reach (black curve) and 95% C.L. exclusion limit (red curve) for 14 TeV LHC with 300 fb^{-1} integrated luminosity, in the $m_{\tilde{b}_1}$-$m_{\chi_1^0}$ plane. For a large range of mass of χ_1^0 (from massless to about 300 GeV), sbottom masses up to about 880 GeV can be discovered and 1050 GeV will be excluded at 95% C.L. if there is no further signal over SM backgrounds being found. The reach at a lower mass of χ_1^0 is better than that of the left-handed case, since lowering the mass of χ_1^0 will increase the p_T of the b-jet produced together with χ_1^0, and this effect is suppressed in the left-handed case where the leading b-jets are produced together with χ_2^0 or χ_1^+ which are always heavier than χ_1^0.

IV. SUMMARY AND CONCLUSION

In this paper, we stress the point that in a realistic situation in a generic MSSM, the sbottom decay can be far from 100% to a specific channel, as assumed in most of the current studies and all the LHC sbottom searches, which is only true for the Bino-LSP and either the left-handed sbottom (or a nearly degenerate stop) being the NLSP or the right-handed sbottom (or Wino) being the NLSP. On a more general ground, sbottom decays lead to a much richer pattern. The inclusion of the other decay channels will significantly weaken the current sbottom search limits and in the meantime open new decay modes for alternative discovery channels for sbottom searches.

We studied in detail the sbottom decay patterns in a few representative SUSY mass scenarios. For the left-handed sbottom, we found the following:

(1) In the Wino-NLSP case [see Fig. 1(a)], $\mathrm{BR}(\tilde{b}_1 \to b\chi_2^0) \sim \mathrm{BR}(\tilde{b}_1 \to t\chi_1^\pm) \sim 50\%$ while $\mathrm{BR}(\tilde{b}_1 \to b\chi_1^0) \sim 2\%$.

(2) In the Higgsino-NLSP case [see Fig. 1(b)], $\tilde{b}_1 \to t\chi_1^\pm$ dominates while $\tilde{b}_1 \to b\chi_{1,2,3}^0$ are all suppressed.

(3) In mixed NLSP cases [see Figs. 1(c) and 1(d)], $\mathrm{BR}(\tilde{b}_1 \to b\chi_2^0) \sim \mathrm{BR}(\tilde{b}_1 \to t\chi_1^\pm) \sim \mathrm{BR}(\tilde{b}_1 \to t\chi_2^\pm) \sim 30\%$ and $\mathrm{BR}(\tilde{b}_1 \to b\chi_1^0) \sim 3\%$ when $|\mu| > M_2$; while $\mathrm{BR}(\tilde{b}_1 \to t\chi_1^\pm) \sim \mathrm{BR}(\tilde{b}_1 \to t\chi_2^\pm) \sim 30\%$ and $\mathrm{BR}(\tilde{b}_1 \to b\chi_1^0) < 10\%$ when $M_2 > |\mu|$.

For the right-handed sbottom (see Fig. 2), decays of $\tilde{b}_1 \to b\chi_1^0$ dominate for the case of Bino-LSP with Wino-NLSP. In the case of Bino-LSP with Higgsino-NLSP, however, the branching fraction of $\tilde{b}_1 \to b\chi_1^0$ is reduced to about 40%–60%, while $\tilde{b}_1 \to t\chi_1^\pm$ is about 20%–30%, followed by $\tilde{b}_1 \to b\chi_{2,3}^0$ of about 10% each.

We analyzed in detail the sbottom pair production signals with the mixed decay channels. We focus on the search sensitivity at the 14 TeV LHC with a 300 fb^{-1} integrated luminosity. We scanned over a large SUSY mass parameter region and performed semirealistic detector simulations. For the left-handed sbottom $\tilde{b}_L$ pair production, we focused on the scenario of Bino-LSP with Wino-NLSP. With one sbottom decaying via $\tilde{b} \to b\chi_2^0$ and the other sbottom decaying via $\tilde{b} \to t\chi_1^\pm$, we found the following:

(i) With $\chi_2^0 \to h\chi_2^0(\mu > 0)$ and $\chi_1^\pm \to W^\pm\chi_1^0$, the leading signal is the $bbbbjj\ell + \not{E}_T$ final state. From Fig. 4(a), we see that a 5σ discovery can be made up to 920 GeV, and the 95% C.L exclusion limit can reach up to 1050 GeV for this Higgs channel. The reach of the combined sbottom and stop signals of the same final states is about 120 GeV higher, as shown in Fig. 4(b).

(ii) With $\chi_2^0 \to Z\chi_2^0(\mu < 0)$ and $\chi_1^\pm \to W^\pm\chi_1^0$, we studied the reach of the $bbjjjj\ell\ell + \not{E}_T$ final state. As seen from Fig. 6, a 5σ discovery can be made up to 840 GeV, and the 95% C.L. exclusion limit can reach up to 900 GeV for the Z channel. The 5σ discovery potential of the combined sbottom and

stop signals can reach up to 980 GeV, and the 95% exclusion limit is about 1025 GeV.

We also studied the signal for the right-handed sbottom $\tilde{b}_R$ in the scenario of Bino-LSP with Higgsino-LSP. With one sbottom decaying via $\tilde{b} \to b\chi_1^0$, and the other sbottom decaying via $\tilde{b} \to t\chi_1^{\pm}$, we found that the reach of $bbjj\ell + \not{E}_T$ final states can lead to a 5σ discovery up to 900 GeV, and the 95% C.L. exclusion limit up to 1060 GeV, as shown in Fig. 7. Including the other commonly studied channels, $b\chi_1^0\bar{b}\chi_1^0$, $b\chi_2^0\bar{b}\chi_2^0$, and $t\chi_1^-\bar{t}\chi_1^+$ would help increase the overall search sensitivity, but we did not repeat the analyses as listed in Table I.

ACKNOWLEDGMENTS

The work of T. H. was supported in part by the U.S. Department of Energy under Grant No. DE-FG02-95ER-40896 and in part by PITT PACC. The work of S. S. and H. Z. was supported by DoE under Grant No. DE-FG02-04ER-41298. The work of Y. W. was supported by Chinese Scholarship Council.

[1] J. L. Feng, Annu. Rev. Nucl. Part. Sci. **63**, 351 (2013).
[2] G. F. Giudice, *Proc. Sci.*, EPS-HEP2013 (2013) 163 [arXiv:1307.7879].
[3] G. Altarelli, Phys. Scr. **T158**, 014011 (2013).
[4] S. P. Martin, Adv. Ser. Dir. High Energy Phys. **21**, 1 (2010).
[5] D. Chung, L. Everett, G. Kane, S. King, J. Lykken, and L. Wang, Phys. Rep. **407**, 1 (2005).
[6] M. Carena, S. Heinemeyer, C. Wagner, and G. Weiglein, Eur. Phys. J. C **45**, 797 (2006).
[7] S. Chatrchyan *et al.* (CMS Collaboration), CERN, Geneva, Technical Report No. CMS-PAS-SUS-13-018, 2014 [http://cds.cern.ch/record/1693164].
[8] G. Aad *et al.* (ATLAS Collaboration), J. High Energy Phys. 10 (2013) 189.
[9] G. Aad *et al.* (ATLAS Collaboration), Phys. Rev. D **90**, 052008 (2014).
[10] E. Alvarez and Y. Bai, J. High Energy Phys. 08 (2012) 003.
[11] H. M. Lee, V. Sanz, and M. Trott, J. High Energy Phys. 05 (2012) 139.
[12] X.-J. Bi, Q.-S. Yan, and P.-F. Yin, Phys. Rev. D **87**, 035007 (2013).
[13] B. Dutta, A. Gurrola, K. Hatakeyama, W. Johns, T. Kamon, P. Sheldon, K. Sinha, S. Wu, and Z. Wu, Phys. Rev. D **92**, 095009 (2015).
[14] M. Adeel Ajaib, T. Li, and Q. Shafi, Phys. Lett. B **701**, 255 (2011).
[15] G. Aad *et al.* (ATLAS Collaboration), J. High Energy Phys. 10 (2014) 24.
[16] S. Chatrchyan *et al.* (CMS Collaboration), CERN, Geneva, Technical Report No. CMS-PAS-SUS-13-008, 2013 [https://cds.cern.ch/record/1547560].
[17] G. Aad *et al.* (ATLAS Collaboration), J. High Energy Phys. 06 (2014) 035.
[18] S. Chatrchyan *et al.* (CMS Collaboration), J. High Energy Phys. 01 (2014) 163.
[19] S. Chatrchyan *et al.* (CMS Collaboration), Phys. Rev. D **90**, 032006 (2014).
[20] A. Belyaev, S. Khalil, S. Moretti, and M. C. Thomas, J. High Energy Phys. 05 (2014) 076.
[21] J. Eckel, S. Su, and H. Zhang, J. High Energy Phys. 07 (2015) 075; J. Eckel, S. Su, and H. Zhang, arXiv:1411.1061.
[22] G. Aad *et al.* (ATLAS Collaboration), J. High Energy Phys. 09 (2014) 015.
[23] G. Aad *et al.* (ATLAS Collaboration), CERN, Geneva, Technical Report No. CERN-PH-EP-2014-143, 2014; J. High Energy Phys. 11 (2014) 118.
[24] G. Aad *et al.* (ATLAS Collaboration), J. High Energy Phys. 06 (2014) 124.
[25] S. Chatrchyan *et al.* (CMS Collaboration), CERN, Geneva, Technical Report No. CMS-PAS-SUS-13-015, 2013 [https://cds.cern.ch/record/1635353].
[26] S. Chatrchyan *et al.* (CMS Collaboration), CERN, Geneva, Technical Report No. CMS-PAS-SUS-14-011, 2014 [https://cds.cern.ch/record/1745586].
[27] S. Chatrchyan *et al.* (CMS Collaboration), Eur. Phys. J. C **73**, 2677 (2013).
[28] S. Chatrchyan *et al.* (CMS Collaboration), CERN, Geneva, Technical Report No. CMS-PAS-SUS-13-009, 2014 [http://cds.cern.ch/record/1644584].
[29] G. Aad *et al.* (ATLAS Collaboration), Eur. Phys. J. C **74**, 2883 (2014).
[30] V. Khachatryan *et al.* (CMS Collaboration), Phys. Lett. B **736**, 371 (2014).
[31] S. Chatrchyan *et al.* (CMS Collaboration), CERN, Geneva, Technical Report No. CMS-PAS-SUS-13-021, 2013 [https://cds.cern.ch/record/1631338].
[32] S. Chatrchyan *et al.* (CMS Collaboration), Phys. Rev. Lett. **112**, 161802 (2014).
[33] M. L. Graesser and J. Shelton, Phys. Rev. Lett. **111**, 121802 (2013).
[34] J. F. Gunion and H. E. Haber, Phys. Rev. D **37**, 2515 (1988).
[35] S. Jung, J. High Energy Phys. 06 (2014) 111.
[36] J. Alwall, R. Frederix, S. Frixione, V. Hirschi, F. Maltoni, O. Mattelaer, H.-S. Shao, T. Stelzer, P. Torrielli, and M. Zaro, J. High Energy Phys. 07 (2014) 079.
[37] T. Sjostrand, S. Mrenna, and P. Z. Skands, J. High Energy Phys. 05 (2006) 026.
[38] J. de Favereau, C. Delaere, P. Demin, A. Giammanco, V. Lemaître, A. Mertens, and M. Selvaggi (DELPHES 3 Collaboration), J. High Energy Phys. 02 (2014) 057.

[39] J. Anderson *et al.*, arXiv:1309.1057.
[40] A. Broggio, A. Ferroglia, M. Neubert, L. Vernazza, and L. L. Yang, J. High Energy Phys. 07 (2013) 042.
[41] W. Beenakker, S. Brensing, M. Krämer, A. Kulesza, E. Laenen, and I. Niessen, J. High Energy Phys. 08 (2010) 098.
[42] M. Cacciari, S. Frixione, M. L. Mangano, P. Nason, and G. Ridolfi, J. High Energy Phys. 09 (2008) 127.
[43] A. Bredenstein, A. Denner, S. Dittmaier, and S. Pozzorini, Phys. Rev. Lett. **103**, 012002 (2009).
[44] A. Lazopoulos, T. McElmurry, K. Melnikov, and F. Petriello, Phys. Lett. B **666**, 62 (2008).
[45] W. Beenakker, S. Dittmaier, M. Krämer, B. Plümper, M. Spira, and P. M. Zerwas, Nucl. Phys. **B653**, 151 (2003).
[46] J. M. Campbell and R. K. Ellis, J. High Energy Phys. 07 (2012) 052.
[47] T. Han, S. Padhi, and S. Su, Phys. Rev. D **88**, 115010 (2013).
[48] C. Lester and D. Summers, Phys. Lett. B **463**, 99 (1999).
[49] A. Barr, C. Lester, and P. Stephens, J. Phys. G **29**, 2343 (2003).
[50] H.-C. Cheng and Z. Han, J. High Energy Phys. 12 (2008) 063.
[51] A. Avetisyan *et al.*, arXiv:1308.1636.